Impact of Ultra-Short Pulsed Laser (USPL) Ablation Process on Separated Loss Coefficients of Grain Oriented Electrical Steels

Manar Nesser, O. Maloberti, E. Salloum, J. Dupuy, S. Panier, C. Pineau, J.-P. Birat, J. Fortin, P. Dassonvalle

Impact of Ultra-Short Pulsed Laser (USPL) Ablation Process on Separated Loss Coefficients of Grain Oriented Electrical Steels

M. Nesser[1], O. Maloberti[2], E. Salloum[1,2], J. Dupuy[3], S. Panier[1], C. Pineau[4], J-P. Birat[5], J. Fortin[1,2], P. Dassonvalle[2]

[1]Laboratoire LTI, IUT d'Amiens, Amiens, 80025, France
[2]SYMADE-UNILASALLE ESIEE-Amiens, Amiens, 80080, France
[3]Multitel a.s.b.l., Mons, 7000, Belgique
[4]IRT-M2P, Metz, 57070, France
[5]IF Steelman, Semecourt, 57280, France

The purpose of this paper is to study the impact of surface laser treatments with ultra-short pulses (Femtosecond laser) on the magnetic properties of Grain Oriented Electrical Steels (GOES) using the two-temperature model for the ablation process[1], [2] **and the magnetic loss separation model of Bertotti. We demonstrated that the hysteresis and excess loss coefficients behave differently depending on the type of laser treatment and its pulse duration (Long Pulse (LP), Short-Pulse (SP) and Ultra-Short Pulse (USP)). We also presented adjusted models to estimate the impact of the USP on the sheet surface in terms of laser energetic quantities; more precisely the groove depth, the plasma maximum temperature, and the peak surface wave pressure were estimated, relative to its nominal value. The latter physical impacts of laser pulses were then correlated to Bertotti's loss coefficients: the static hysteresis loss coefficient and the excess loss coefficient. The laser process is not always able to reduce simultaneously both loss contributions. Thus, a compromise must be found to optimize the process. The variation of the flux density level as a function of the applied magnetic field was measured with a single sheet tester SST under a one-directional field parallel to the rolling direction. From these measurements, we deduced the whole power loss contributions. Results showed that an optimization of the laser's parameters ensured an iron loss reduction at 50 Hz up to -30% for an induction below 0.5T, and a percentage close to -15% for an induction above 1.5T.**

Index Terms— **Electrical steels, Bertotti's Loss Coefficients, Grain Oriented, Laser Ablation, Power Loss.**

I. Introduction

Pulsed Laser (PL) technology is a recent technique used to optimize the electromagnetic properties of Grain Oriented Electrical Steels (GOES) forming the cores of transformers and chokes [3]. Like the Continuous Wave process, the long and Short Pulsed Laser (SP) processes have been largely studied[4], [5]. The Ultra-Short Pulsed Laser (USPL) ablation technique remains unfamiliar for these electrical steels and its deterministic impact on the performance of these materials requires deep investigations. The classical approach to estimate the temperature variation at the sheet surface is not valid because of the ultra-short pulses used which typically create a non-equilibrium temperature state. A two-temperature model is chosen in this case [1]. The key objective is to interpret and optimize the impact of UPSL process on the magnetic properties of GOES sheets. To do so, the effect of laser energy contributions delivered on the sample surface is presented in terms of plasma electron temperature, shock wave peak pressure and ablated groove depth. These variables are correlated to the magnetic properties of the sample. A Single Sheet Tester (SST) is used to measure the power loss before and after the laser processing and the separated losses are deduced using the Bertotti model. A comparative study of the impact of laser treatment with long, short, and ultra-short pulses on the separated losses is also investigated.

II. Methodology

A. Material and Laser Process

The full study was carried out on commercial Fe-(3wt%)Si grain-oriented squared sheets with a side length of 150 mm and a thickness of 0.23 mm, and a typical grain size of between 15 and 30 mm.

The surface treatment was executed using two different laser equipment giving pulse durations of various orders of magnitude ranging from nanoseconds to femtoseconds (see Table 1). The nanosecond laser used is an IPG pulsed ytterbium fiber laser operating at a wavelength of 1.064 µm. It delivers pulse duration between 4 ns (Short Pulse SP) and 200 ns (Long Pulse LP)[4]. Yet, the femtosecond laser involved is an Ytterbium Amplitude Laser (Ultra-Short Pulse USP) which operates at a wavelength of 1.03 µm with an adjustable pulse width between a few hundreds of fs and 10 ps.

B. Experimental Measurements

The spot size, the laser pattern and its surface density were fixed and kept identical for all experiments with the one-pass process and during the treatment for all samples [5]. Only the pattern density of the two-pass ablation process was different and divided by two. The profile of the grooves on the sample surface was collected by a conventional optical microscope (confocal microscope); the width and depth of the laser line and the reliefs formed were measured.

The variable parameters of each laser configuration are summarized in the following energy quantities: pulse energy density or laser fluence (e_{pulse}) in J·cm^{-2}, peak power density ($\hat{P}$) in TW·cm^{-2}, number of single-pulses (including the overlap) (N) and cumulative energy density (e_{cum}) in J·cm^{-2}. The latter takes into account the number of laser passes and the overlap (see Figure 1).

Once the treatment was performed, we measured the power loss of each treated sample using a single sheet tester (SST).

In the following, we focused on two particular investigations: the impact of ablation on GO samples using a femtosecond laser with a various set of parameters (see Table 2) and the comparison between different types of laser processing by varying the pulse duration between nanosecond and femtosecond. In our study a pulse duration with some

hundreds of femtoseconds leads to the ablation effect, some nanoseconds result in the scribing effect, and some hundreds of nanoseconds result in the irradiation effect [4]. The three different pulse widths studied are defined by the energy contributions delivered by the laser in each case in Table 3.

TABLE I
CHARACTERISTICS OF EACH LASER

Laser Type	Wavelength	Pulse duration
Laser LPL*	1.064 µm	100 ns – 200 ns
Laser SPL*	1.064 µm	4 ns – 30 ns
Laser USPL*	1.03 µm	500 fs – 10 ps

*LPL: Long Pulsed Laser, SPL: Short Pulsed L., USP: Ultra-Short Pulsed L..

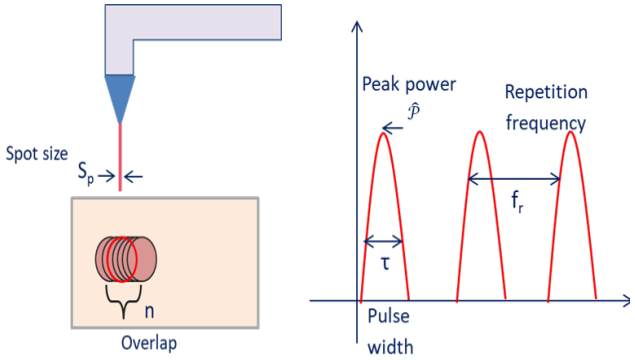

Fig. 1. Schematic of the Laser Beam and Pulse Characteristics.

TABLE 2
LASER ABLATION PARAMETERS USED IN TERMS OF ENERGY CONTRIBUTIONS

Config.	$\hat{P}$ TW·CM^{-2}	e_{pulse} J·CM^{-2}	E_{cum} J·CM^{-2}	N_{pass}	N
Abl_1	23.4	11.71	1171.3	1	100
Abl_2	23.4	11.71	2342.7	2	100
Abl_3	23.4	5.09	509.30	1	100
Abl_4	10.2	5.09	50.93	1	10
Abl_5	30.5	15.28	1527.8	1	100

TABLE 3
LASER PARAMETERS USED FOR DIFFERENT TYPE OF TREATMENT IN TERMS OF ENERGY CONTRIBUTIONS

Laser Type	$\hat{P}$ MW·CM^{-2}	e_{pulse} J·CM^{-2}	E_{cum} J·CM^{-2}	N_{pass}
LPL* (Irr)	12.73	1.27	509.3	1
SPL* (Scr)	127.32	0.51	509.3	1
USPL* (Abl_2)**	23.4 e^6	11.71	2342.7	2

*LP: long pulse duration, SP: short pulse duration, USP: ultra-short pulse duration. **The ablation configuration resulting in best power loss reduction

III. MODELING

A. Bertotti Coefficients Calculation

For a detailed analysis of the measured losses, we applied the Bertotti loss separation model [6] to identify the impact of different laser treatments on each loss component which should help understand the physics behind each phenomenon. The total loss density per unit mass is given by the following empirical formula:

$$P_{tot} = k_h.f.B^2 + k_c.f^2.B^2 + k_e.f^{1.5}.B^{1.5} \quad (1)$$

Where f is the frequency and B is the induction level or flux density. The main parameters of Bertotti's model are the hysteresis loss coefficient k_h $[J.kg^{-1}.T^{-2}]$, the classical loss coefficient k_c $[J.s.kg^{-1}.T^{-2}]$ and the excess loss coefficient k_e $[J.s^{1/2}.kg^{-1}.T^{-3/2}]$. k_c, the classical eddy current loss coefficient is proportional to the electrical conductivity σ and the rolling thickness e and inversely proportional to the material density ρ according to the following relationship:

$$k_c = \frac{e^2 \pi^2 \sigma}{6 \rho} \quad (2)$$

The eddy current coefficient k_c is a constant identified based on the material properties and thickness (see Equation (2)). The hysteresis loss coefficient k_h was deduced from the total loss measured at a very low frequency (3 Hz) for which the classical eddy current loss and the excess loss are negligible. Then, providing k_h and k_c are known, using the loss separation equation (1), the excess loss coefficient k_e was determined as a function of the induction level B and frequency f using the total power loss provided by the experimental data.

B. Laser Ablation Model

Understanding the influence of the USPL surface treatment on material properties is helpful to guide us optimizing this effective treatment. To do so, we have established the relationships between the laser energy parameters and their effects on the surface; in terms of plasma electron temperature or shock wave peak pressure and groove depth.
Thus, considering the laser-matter interaction within the femtosecond time scale the energy accumulated by the free electrons is transferred to the lattice by collisions, causing it to heat up to the point of sublimation. The free electrons absorb the laser energy very quickly, lasting a few tens of femtoseconds, while their relaxation in the lattice varies between 1 and 10 ps. The pulse duration is shorter than the cooling time of the electrons. The use of ultra-short pulses shorter than these transfer times implies a decoupling between the thermal behavior of the electrons at temperature T_e and the thermal behavior of the lattice at temperature T_l [2],[1].
Consequently, the classical approach to estimate a temperature is not valid. This non-equilibrium temperature state is expressed by the two-temperature model which involves both the electron temperature and the lattice temperature. The electron temperature T_e and the ablation depth p from the energy quantities of each laser configuration were estimated based on the literature [1],[2]. First, the electron temperature achieved during the laser ablation process is estimated using the following equation (3):

$$T_e \simeq \left(\frac{2 \cdot A_0 \cdot e_{pulse} \cdot \alpha}{C_e'}\right)^{\frac{1}{2}} \quad (3)$$

The absorption rate of ferrous metal A_0 is about 35% at a wavelength of about 1 µm [5], but should be nonlinear and depend on the laser power and ablated groove profile. e_{pulse} is the laser fluence. C_e' is the electron heat capacity coefficient per unit volume ($C_e = C_e' T_e$, $C_e' \approx 84\, J.m^{-3}.K^{-2}$) and α is an optical penetration depth $\alpha = \frac{\rho \cdot \Delta Hfe}{e_{th}}$ [m^{-1}] with ρ the metal density, ΔHf_e is the specific heat of evaporation and e_{th} is the threshold fluence for ablation (it equals approximately 0.5 J·cm^{-2} for FeSi [1]). Then, the ablation depth of N pulses

($N_{pass}=1$ for single pass and $N_{pass}=2$ for double pass) as a function of the laser fluence is estimated using the following expression (4):

$$p \simeq e_i + N * N_{pass} * \alpha^{-1} ln\,(A_0 * e_{pulse}/e_{th}) \quad (4)$$

where e_i is the insulating coating (automatically removed during the ablation process).

In parallel to the groove depth and electron temperature, we estimated the shock wave peak surface pressure as a function of the laser peak power with a shock wave model. A simple shock wave model was well developed by Peyre and Fabbro [7]. It estimates the residual stress induced in the metal sheet subjected to a short laser pulse with specified laser power density, pulse width, and spot size. In this model, they calculated the pressure generated by the plasma in the metal substrate during the laser ablation process. Hence, the plasma layer formed during the ablation process induces a shock wave and a compression pressure leading to local plastic deformation and a residual stress field in the localized volume of the laser spot. The value of the pressure (*Pr*) generated is proportional to the square root of the peak power density ($\hat{P}$):

$$\mathrm{Pr} = \mathrm{BC} * \hat{P}^{\frac{1}{2}} \quad (5)$$

Pr in kbar and $\hat{P}$ in GW·cm^{-2}, *BC* is a constant depending on the confinement layer (BC=10 for water confinement). The pressure generated in the case of ablation with a confinement layer is greater with one order of magnitude than for direct ablation. In our case, the laser beam is applied directly on the material surface, so the value of BC is considered close to 1.

The plastic deformation and the creation of dislocations in the material occur only if the magnitude of the primary shockwave is higher than the dynamic yield strength or the Hugoniot Limit. During the propagation of the wave, the volume affected is plastically strained, thus after the interaction, the surrounding material induces biaxial compressive residual stresses on the plane parallel to the surface, to oppose the straining only if the value of peak stress exceeds the Hugoniot limit. Using the femtosecond laser with high peak power induces a peak pressure that exceeds the Hugoniot limit but the theoretical value of the plastically affected depth might be small due to the very short pulse duration. Thus, the shock wave created shouldn't propagate deeply into the material. However, we still can estimate the surface peak pressure (5) and study its behavior as a function of the laser peak power density, because it has got an impact on the surface magnetic domains.

IV. Results

A. Total Power loss Variation

Following the different types of laser treatment – irradiation, scribing and ablation - the total losses of each sample are collected using the single sheet tester (SST). We considered the values of power loss reduction at four induction levels (0.1 T, 0.5 T, 1 T, and 1.5 T) for the 50 Hz frequency. Then, we selected one irradiation configuration with the LP laser, a scribing configuration with the SP laser, and the ablation configuration with the USP laser (Abl_2). The latter is a two-pass laser ablation configuration. The energy contributions of each configuration are detailed in Table 3.

TABLE 4
PERCENTAGE OF TOTAL POWER LOSSES VARIATION UNDER LASER TREATMENT

Induction at 50 Hz	LASER LPL (IRR) % ΔP	LASER SPL (SCR) % ΔP	LASER USPL (ABL_2) % ΔP
1.5 T	-11.3	-11.0	-13.6
1 T	-9.8	-11.9	-21.3
0.5 T	-18.6	-17.8	-38.1
0.1 T	-11.7	-7.5	-58.7

The percentage of loss variation of each sample is calculated relative to the same sample before and after laser treatment.

The percentage of total losses variation presented in Table 4 shows that the USP laser ablation configuration (Abl_2) provides a loss reduction higher than that achieved using laser irradiation or scribing. This loss reduction reached 13% for the 1.5T induction at 50 Hz and a maximum value of 38% at 0.5T for a frequency of 50 Hz.

B. Behavior of Separated Losses (Bertotti Coefficients)

An extensive analysis of power losses was carried out to understand the origin of the loss reduction and its connection to the laser pulse duration. Applying the Bertotti model, a separated losses study showed that the contribution of each loss component varies with the induction level and frequency and with the type of laser treatment. Respectively, in order to identify at a given induction *B* and frequency *f* level which component among the hysteresis losses and the excess losses is in the majority, it is necessary to compare $k_h\sqrt{B}$ to $k_e\sqrt{f}$. We calculated the percentage of change in the hysteresis loss coefficient k_h and the excess loss coefficient k_e of the treated sample according to its value before laser treatment and then displayed the results following the laser treatment with a long pulse (irradiation "Irr"), a short pulse (scribing "Scr") and an ultra-short pulse (ablation with two configurations "Abl_1" and "Abl_2") in Figure 2. Notably, the use of laser irradiation configuration "Irr" reduced significantly the hysteresis loss coefficient k_h at different induction levels for frequency 50 Hz whereas it slightly decreased the excess loss coefficient. It must be noticed that the scribing configuration behaves in a like manner as the irradiation configuration with a higher reduction for the excess loss coefficient. However, for ablation, we deduced that if the treatment is done with the same pattern density with one-pass the effect on the hysteresis loss and the excess loss coefficients was similar at high induction, both were reduced. While, the ablation in two-pass with a lower pattern density resulted in the highest decrease in both coefficients, especially that of excess loss.

The variation of the hysteresis and excess loss coefficients is dependent on the type of laser treatment which asserts that a laser treatment acts differently on the sample surface depending on the laser type and its pulse duration:

The long pulses of the order of nanoseconds with small grooves and located induced thermal stresses could allow the generation of misoriented 90° closure domains at the vicinity of the laser spots which shows a significant reduction of the hysteresis loss coefficient without a significant impact on the excess loss coefficient related to the dynamics and mobility of the wall. The hysteresis loss coefficient is proportional to the

defect density responsible for the wall pinning effect, partly due to the magnetic poles and demagnetizing effect around these defects. In the cases of irradiation and scribing, magnetic poles and demagnetizing effect are minimized thanks to the misoriented 90° closure domains appearing due to the thermally induced stress anisotropy. On the other hand, ultra-short pulses with duration of the order of a few hundreds of femtoseconds with an ablation effect that produces a deep groove in the sheet can generate different kinds of defects with magnetic poles that can pin the walls which is not favorable to the hysteresis coefficient especially at low induction levels. However, it can help the domain wall nucleation and 180° closure domains multiplication at the vicinity of the laser lines and facilitate the process of magnetization at higher induction levels. The most typical effect is also the 180° magnetic domain refinement and a change in the wall's mobility. The excess loss coefficient is inversely proportional to walls density and mobility and therefore shows a greater reduction after ablation.

C. Estimated Variables of Laser Ablation Model

The behavior of the estimated groove depth and electron temperature is presented in Table 5, it is showed that both these variables increased as a function of the cumulative energy density and pulse energy. As mentioned in the modeling section, the use of the femtosecond laser with high peak power induces a peak pressure that overpasses the Hugoniot limit, but the theoretical value of the plastically affected depth might be very small and insignificant due to the ultra-short pulse duration. Thus, the shock wave created should not propagate into the material but modify the surface induced stress and the magnetic structure. Thus, we limited this model on the estimation of the surface peak pressure, which showed an upward behavior as a function of the laser peak power density. In the following subsection, we studied the behavior of the magnetic parameters as a function of the estimated relative laser impact values: the electron temperature T_e, the peak pressure Pr and the ablation depth p (relative to its nominal values $T_{e,n}$, Pr_n and p_n).

TABLE 5
THE ESTIMATED ELECTRON TEMPERATURE, GROOVE DEPTH AND PEAK PRESSURE FOR EACH ABLATION CONFIGURATION

Config.	$\hat{P}$ TW·CM^{-2}	e_{pulse} J·CM^{-2}	E_{cum} J·CM^{-2}	$T_e/T_{e,n}$	p/p_n	Pr/Pr_n
Abl_1	23.4	11.71	1171.3	1.60	0.83	1.53
Abl_2	23.4	11.71	2342.7	1.60	1.53	1.53
Abl_3	23.4	5.09	509.30	1.06	0.27	1.01
Abl_4	10.2	5.09	50.93	1.06	0.14	1.01
Abl_5	30.5	15.28	1527.8	1.83	1.00	1.75

D. Correlations and Discussion

To correlate between the estimated variables corresponding to the ablation impact on the sample surface and the calculated magnetic parameters, we presented the variation of Bertotti coefficients as a function of calculated relative groove depth (p/p_n), the relative plasma electron temperature ($T_e/T_{e,n}$), and the relative shock wave peak pressure (Pr/Pr_n).

Since the electron temperature is proportional to the square root of the fluence and the peak pressure is proportional to the square root of the peak power density, *i.e.* also the fluence, the study as a function of these two parameters is similar and the magnetic properties showed the same behavior as a function of these physical impacts (Figure 3). This observation has been physically coherent since there is a close relationship between the temperature and the pressure even within a plasma gas.

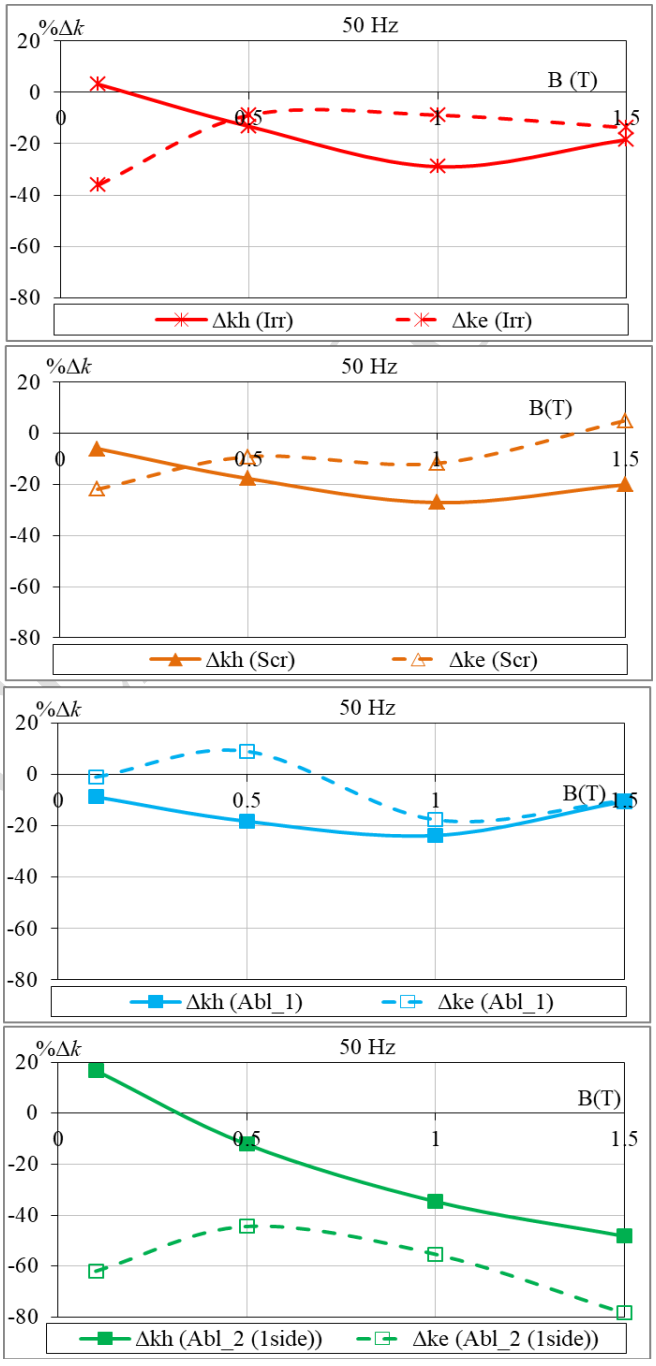

Fig. 2. Variation of Bertotti's Coefficient k_h and k_e as a Function of the induction level, at frequency 50Hz, for Different Laser Treatments.

For a peak induction of 1.5 T at a frequency of 50 Hz, the groove depth-dependent excess loss coefficient seemed to be a monotonously decreasing function (Figure 4), but the hysteresis loss coefficient had got a minimum and increased for deeper grooves. Grooves in the metal previously meant defects and walls pinning effect with always an increase of hysteresis loss coefficients. On the contrary, in the case of

ablation, the grooves in the metal could behave as nucleation centers rather than pinning centers, probably thanks to the engraving done with ultra-short pulses and without thermal effect. Such "clean" grooves might give rise to located magnetic poles and 180° spike-like domains rather than various misoriented 90° closure domains and Lancet domains.

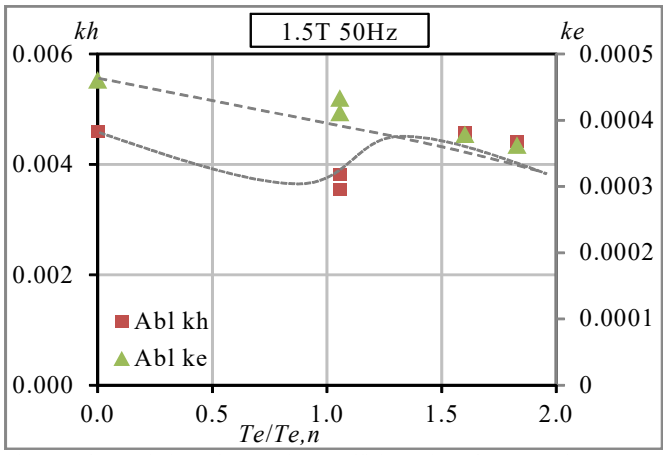

Fig. 3. The Variation of Bertotti's Coefficients k_h and k_e per unit mass as a function of the relative electron temperature $T_e/T_{e,n}$ (or Peak Pressure Pr/Pr_n which provides identical curves) at induction 1.5T and the frequency 50Hz.

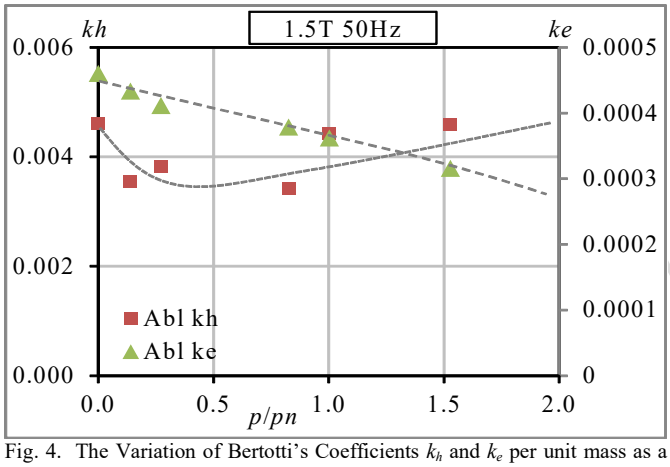

Fig. 4. The Variation of Bertotti's Coefficients k_h and k_e per unit mass as a function of the relative Groove Depth p/p_n at induction 1.5T and the frequency 50Hz.

Therefore, deep grooves in the metal refine the magnetic domains significantly while reducing the dynamic losses, while the inclusion of such deep grooves adds defects increasing the hysteresis losses. As a consequence, a compromise with a specific optimal depth (the nominal value p_n) for the grooves must be found. The chief advantage of the ablation process seems to be the minimization of thermal effect which permits to reduce more significantly the excess loss coefficient. It should always be possible to engrave two identical grooves with two different ultra-short pulses. Therefore, the dependence of the magnetic properties should be studied not only on the groove depth but also on the electronic plasma temperature T_e or the peak pressure Pr of the shock wave. It showed an optimal value for a temperature and a peak pressure close to the corresponding nominal values $T_{e,n}$ and Pr_n beyond which thermal and mechanical induced effects start to increase the hysteresis loss coefficient higher than the dynamic losses at 50 Hz. Having higher temperature or pressure may be interesting only at lower induction levels and higher frequencies for which the static hysteresis loss is negligible in front of the dynamic losses. In this case, the limitation is the mechanical weakening or deformation of the sheet and the necessity to magnetize the material up to 1.5 T because the permeability can be then lower than initially.

V. Conclusion

The influence of laser pulse duration (long, short and ultra-short pulse) on the magnetic properties of grain-oriented FeSi electrical steel sheets was developed. Using Bertotti model, we identified loss coefficients based on the total power losses measured with the Single Sheet Tester (SST). We conclude that each type of laser treatment behaves differently on the separated loss components. Consequently, the use of a laser with ultra-short pulse duration provides the highest reduction rate for the dynamic loss component. Moreover, the laser-matter interaction in the case of the ultra-short pulsed laser is studied by a two-temperature model to derive the groove depth and the plasma electron temperature. Also, using the shock-wave model, an estimate of the peak pressure has been made. The correlation between these estimated laser impacts and the separated loss coefficients led to an optimization of these values ensuring a reduction in total losses.

Acknowledgment

This research has received funding from the European Research Council under the H2020-IND-CE-2016-17/H2020-FOF-2017 Program (Grant No. 766437).

References

[1] K. H. Leitza, B. Redlingshöfer, Y. Reg, A. Otto, et M. Schmidt, « Metal Ablation with Short and Ultrashort Laser Pulses », *Phys. Procedia*, vol. 12, p. 230-238, 2011, doi: 10.1016/j.phpro.2011.03.128.

[2] B. N. Chichkov, C. Momma, S. Nolte, F. Alvensleben, et A. Tünnermann, « Femtosecond, picosecond and nanosecond laser ablation of solids », *Appl. Phys. Mater. Sci. Process.*, vol. 63, nº 2, p. 109-115, août 1996, doi: 10.1007/BF01567637.

[3] I. Petryshynets, F. Kováč, V. Puchý, M. Šebek, J. Füzer, et P. Kollár, « Magnetic losses reduction in grain oriented silicon steel by pulse and continuous fiber laser processing », *AIP Adv.*, vol. 8, nº 4, p. 047604, avr. 2018, doi: 10.1063/1.4994191.

[4] M. Nesser *et al.*, « Correlation between laser energetic parameters and magnetic properties of GO laminations under surface treatments with long, short or ultra-short pulsed lasers », *J. Magn. Magn. Mater.*, vol. 504, p. 166696, juin 2020, doi: 10.1016/j.jmmm.2020.166696.

[5] J. Dupuy, M. Nesser, O. Maloberti, et Y. Hernandez, « Comparison between laser thermal effects and ablation effects with ultrashort pulses laser on GO SiFe electrical steel », *Proc SPIE 10911 High-Power Laser Mater. Process. Appl. Diagn. Syst. VIII*, vol. 10911, p. 1091104, 2019, doi: 10.1117/12.2505326.

[6] G. Bertotti, « General properties of power losses in soft ferromagnetic materials », *IEEE Trans. Magn.*, vol. 24, p. 621-630, 1988, doi: 10.1109/20.43994.

[7] P. Peyre et R. Fabbro, « Laser shock processing: a review of the physics and applications », *Opt. Quantum Electron.*, vol. 27, p. 1213-1229, 1995, doi: 10.1007/BF00326477.